Chinese Chemical Letters 31 (2020) 1168–1172

Contents lists available at ScienceDirect

Chinese Chemical Letters

journal homepage: www.elsevier.com/locate/cclet

Communication

NIR light-induced tumor phototherapy using ICG delivery system based on platelet-membrane-camouflaged hollow bismuth selenide nanoparticles

Kaili Ding[a], Cuixia Zheng[a], Lingling Sun[a], Xinxin Liu[a], Yanyan Yin[b,**], Lei Wang[a,c,*]

[a] School of Pharmaceutical Sciences, Zhengzhou University, Zhengzhou 450001, China
[b] School of Pharmacy, Xinxiang Medical University, Xinxiang 453000, China
[c] Key Laboratory of Targeting Therapy and Diagnosis for Critical Diseases, Zhengzhou 450001, China

ARTICLE INFO

Article history:
Received 27 August 2019
Received in revised form 29 October 2019
Accepted 30 October 2019
Available online 4 November 2019

Keywords:
Platelet membrane
Biomimetic nanoplatform
Photothermal therapy
Tumor-targeting
Near-infrared laser irradiation

ABSTRACT

Near-infrared (NIR) light-triggered photothermal therapy (PTT) is a promising treatment strategy for treating cancer. The combination of nanotechnology and NIR has been widely applied. However, the therapeutic efficacy of the drug-delivery system depends on their ability to avoid phagocytosis of endothelial system, cross the biological barriers, prolong circulation life, localize and rapidly release the therapeutic at target sites. In this work, we designed a platelet membrane (PM)-camouflaged hollow mesoporous bismuth selenide nanoparticles (BS NPs) loading with indocyanine green (ICG) (PM@BS-ICG NPs) to achieve the above advantages. PM-coating has active tumor-targeting ability which could prevent drug leakage and provide drug long circulation, causing drug delivery systems to accumulate in tumor sites effectively. Moreover, as a type of the photothermal sensitizers, BS NPs are used as the inner cores to improve ICG stability and are served as scaffolds to enhance the hardness of this drug delivery system. For one hand, the thermal vibration of BS NPs under NIR laser irradiation causes tumor inhibition through hyperthermia. For another hand, this hyperthermia process could damage PM and let ICG rapid release from PM@BS-ICG NPs. The *in vitro* and *in vivo* results showed that this biomimetic nano-drug delivery system exhibits obvious antitumor activity which has good application prospect.

Photothermal therapy (PTT), as one of the promising approaches in cancer therapy, offers spatiotemporally controlled tumor treatment with minimal invasiveness [1–3]. PTT ablates tumor through the rapid heating generated based on the photosensitizers with laser irradiation [4–6]. It is reported that ICG could be used for PTT, however, there are several intrinsic drawbacks of it, such as instability, rapid clearance in the body, being prone to self-bleaching and lack of targeting ability in human body [7–9]. In order to address these issues, new carriers need to be constructed for ICG loading [10–13].

Nowadays, Bi_2Se_3 nanoparticles (BS NPs), especially the hollow mesoporous form, have attracted the attention of the researchers. Yu *et al.* [14] have developed a bismuth selenide spherical sponge nano-drug delivery platform to achieve photothermal therapy of tumors. Zhang *et al.* [15] employed macrophage membrane to encapsulate hollow BS to prepare a biomimetic nano-drug delivery system which successfully inhibited lung metastasis of breast cancer. Compared with other drug delivery victors [16–21], BS NPs not only have high drug-loading ability and biodegradability, but also have comparative characteristics of CT/photoacoustic imaging [22–25]. Bi has higher X-ray attenuation [Bi > Au > Pt > Ta > I at 100 keV], which is an environmentally friendly element that can be excreted through the kidney [26]. Moreover, Se is known as the "king of anti-cancer" of trace elements in human body [27]. This means BS NPs can be used as not only sensitizers for PTT, but also as drug carriers for ICG loading. However, the conventional inorganic NPs were severely restricted owing to the rapid clearance by the reticuloendothelial systems (RES) or phagocyte system (such as macrophages) [28,29].

In recent years, biomimetic nano-drug delivery system is becoming a hotspot due to its inherent biocompatibility, biodegradability and non-immunogenicity. Researchers have used multiple types of cell membranes, including erythrocyte membrane [30],

* Corresponding author at: School of Pharmaceutical Sciences, Zhengzhou University, Zhengzhou 450001, China.
** Corresponding author.
E-mail addresses: yinyanyan@xxmu.edu.cn (Y. Yin), wanglei1@zzu.edu.cn (L. Wang).

https://doi.org/10.1016/j.cclet.2019.10.040
1001-8417/

leukocyte membrane [31], tumor cell membrane [32], platelet membrane [4] *etc.*, to disguise the NPs, bypass the immune system recognition and maximize the drug accumulation in tumor sites. Platelet is an indispensable component of blood stream with the ability of targeting vascular injury sites to impede thrombogenesis and maintain the integrity of blood circulation [33]. Recent studies have shown that platelet-disguised NPs have multiple functions, such as selective adhering injured blood vessels [20], clearing bacteria [21], targeting atherosclerotic tissue [22], *etc*. Moreover, the P-selectin proteins expressed on the surface of platelet membranes can specifically bind to the CD44 receptors on the surface of cancer cells [33]. Therefore, it is significant to construct a platelet-membrane-cloaked nano-system with active tumor cell-targeting.

Herein, platelet membrane (PM)-camouflaged BS NPs with ICG-loading (PM@BS-ICG NPs) were constructed for tumor therapy. PM was used as the outer shell which provided the advantages of excellent biocompatibility, long circulation and active tumor-targeting. As the inner cores, BS-ICG NPs not only have high ICG loading capacities, but also enhance photothermal therapeutic efficacy. In general, we hypothesized that the PM@BS-ICG NPs could actively target to tumor sites and sequentially deliver anticancer therapeutics to their most active destinations.

The PM@BS-ICG NPs were synthesized and characterized with the following steps. Firstly, Bi_2O_3 NPs were prepared and the transmission electron microscopy (TEM) result showed that the NPs were spherical and homogeneous with an average diameter of ~100 nm (Fig. 1a). Subsequently, hollow mesoporous BS NPs were prepared using Bi_2O_3 NPs as template and precursor *via* the hydrothermal method [34]. The TEM result (Fig. 1b) revealed their well hollow mesoporous structures with an average diameter of ~110 nm. The pore size and specific surface area were measured to be ~8.96 nm and 71.3 m^2/g, respectively, according to N_2 adsorption-desorption isotherms (Fig. 1c). Besides, the Fourier Transform Infrared Spectrometer (FT-IR) was used for further determination (Fig. 1d). The absorption peak at 3420 cm^{-1} was assigned to O—H stretching vibration. Moreover, the characteristic adsorption peak of C=O stretching vibration was located at 1870 – 1540 cm^{-1}. The adsorption bands of stretching vibration and bending vibration of CH were at 3000 – 2850 cm^{-1} and 1480 – 1350 cm^{-1}, respectively. What is more, the absorption peak at 1100 – 1000 cm^{-1} was assigned to C—O stretching vibration. These above results showed that organic coatings of glucose decomposition stably existed on the surface of the NPs, demonstrating that hollow BS NPs were successfully synthesized. Then, ICG was chosen to be encapsulated into BS NPs. Ultraviolet–visible spectrophotometer (UV–vis) absorption spectrum of BS-ICG showed a new broad peak between 600 nm and 800 nm (Fig. 2a), indicating that ICG was loaded into BS NPs. The entrapment efficiency and loading capacity of ICG reached to ~76% and ~13%, respectively. Finally, PM@BS-ICG NPs exhibited a typical core–shell structure and were spherical in shape with good monodispersity (Fig. S1a in Supporting information). The dynamic light scattering (DLS) data of the NPs before and after PM coating were also investigated (Fig. 2b) for further confirmation. Compared with BS-ICG NPs, PM@BS-ICG NPs exhibited a relative increase of ~15 nm in hydrodynamic diameter while their surface zeta-potential were close to the zeta potential of PM (Fig. 2c). And the entrapment efficiency was not significantly changed when they were coated with platelet membrane (Fig. S1b in Supporting information). To further demonstrate that the PM had coated on BS-ICG outside, the membrane proteins in PM and PM@BS-ICG were analysis by salt-polyacrylamide gel electrophoresis (SDS-PAGE). Compared with PM, Fig. S1c (Supporting information) showed that PM@BS-ICG displayed similar protein brands, evidencing the existence of PM proteins in our obtained PM@BS-ICG sample. It has been reported that P-selectin overexpressed on the PM which has a specific and strong affinity with the CD44 receptor. Therefore, western blot was conducted to test the protein on PM and PM@BS-ICG. The result demonstrated that PM@BS-ICG maintained the high expression of P-selectin, similarly to PM (Fig. S1d in Supporting information). Next, we used flow cytometry to determine the expression of CD44 receptors on the B16-F10 cell surface. As shown in Fig. S1e (Supporting information), CD44 receptors were expressed on the surface of the cell.

The photothermal performance of BS NPs was investigated with NIR laser irradiation (808 nm, 2 W/cm^2) for 4 min at different concentrations (0.1, 0.25, and 0.5 mg/mL in PBS). The high thermal

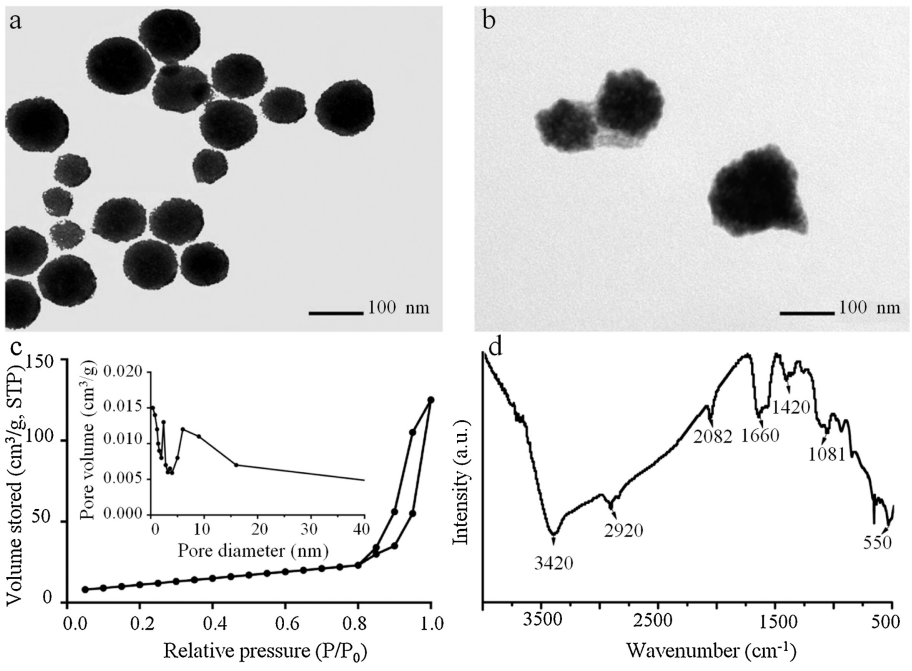

Fig. 1. TEM of Bi_2O_3 NPs (a) and BS NPs (b). (c) N_2 adsorption-desorption isotherm of BS NPs (inset shows the corresponding pore size distribution). (d) FT-IR spectrum of BS NPs.

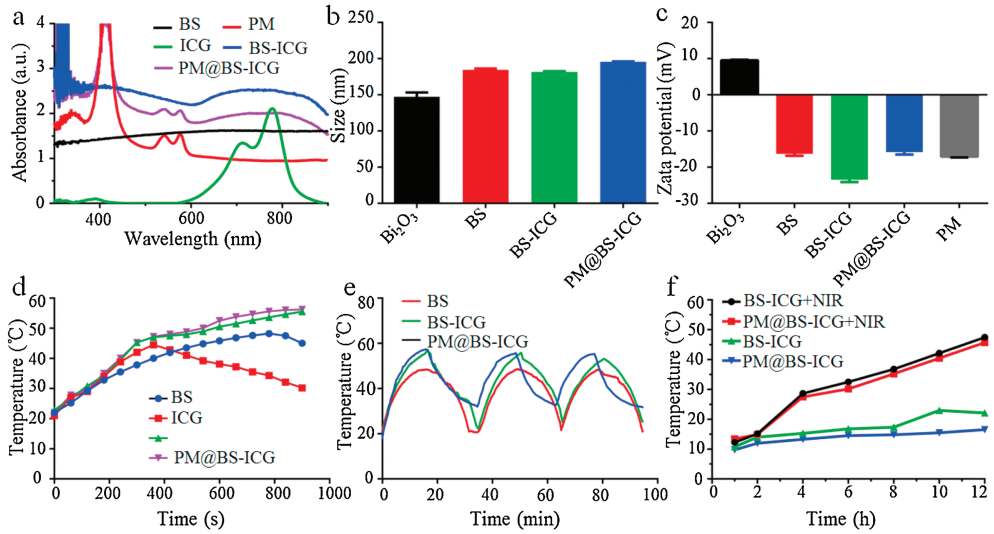

Fig. 2. (a) UV–vis absorption spectra, (b) hydrodynamic size and (c) surface charge of Bi_2O_3 NPs, BS NPs, BS-ICG NPs, PM@BS-ICG NPs. (d) Temperature increases and (e) photostability of BS, BS-ICG, and PM@BS-ICG during NIR laser irradiation. (f) *In vitro* release of ICG from BS-ICG and PM@BS-ICG with or without NIR.

contrast produced by BS NPs (Fig. S2a in Supporting information) proved the high infrared radiation thermal imaging properties. Subsequently, we studied the photothermal effect of ICG. Under 808 nm laser irradiation, the temperature of ICG rapidly rose to ~44.5 °C in 6 min, but its photothermal conversion efficiency was poor and unstable (Figs. S2b and S2c in Supporting information). Besides, we studied the photothermal of BS, BS-ICG and PM@BS-ICG NPs, respectively. As exhibited in Figs. 2d and e, BS-ICG NPs and PM@BS-ICG NPs showed higher thermal effect and remarkable stability when they were irradiated with NIR laser (808 nm, 2 W/cm^2).

Next, we studied the ICG release behavior of PM@BS-ICG NPs with or without NIR laser. As shown in Fig. 2f, after irradiation for 4 min, ICG can be rapidly released from BS-ICG NPs and PM@BS-ICG NPs, which might own to membrane disruption and accelerated thermal vibration caused by the rapid increase of local temperature produced by BS NPs under laser irradiation [24]. The release behavior might be beneficial to reduce the side effects of anti-cancer drugs and enhance the anti-cancer effect.

The *in vitro* cytotoxicity BS NPs with or without NIR irradiation against B16-F10 cells was evaluated by using CCK-8 method [15]. As showed in Fig. 3a, BS NPs exhibited negligible cytotoxicity to B16-F10 cells even at a concentration of 120 μg/mL. In contrast, the viability of B16-F10 cells treated with BS NPs declined sharply after 2 min irradiation with an 808 nm laser (2 W/cm^2). Then, the photothermal effect of BS NPs on cells was detected by Calcein-AM/PI assay [35]. PI can only stain apoptotic/dead cells with red fluorescence, and Calcein-AM can only stain the living cells with

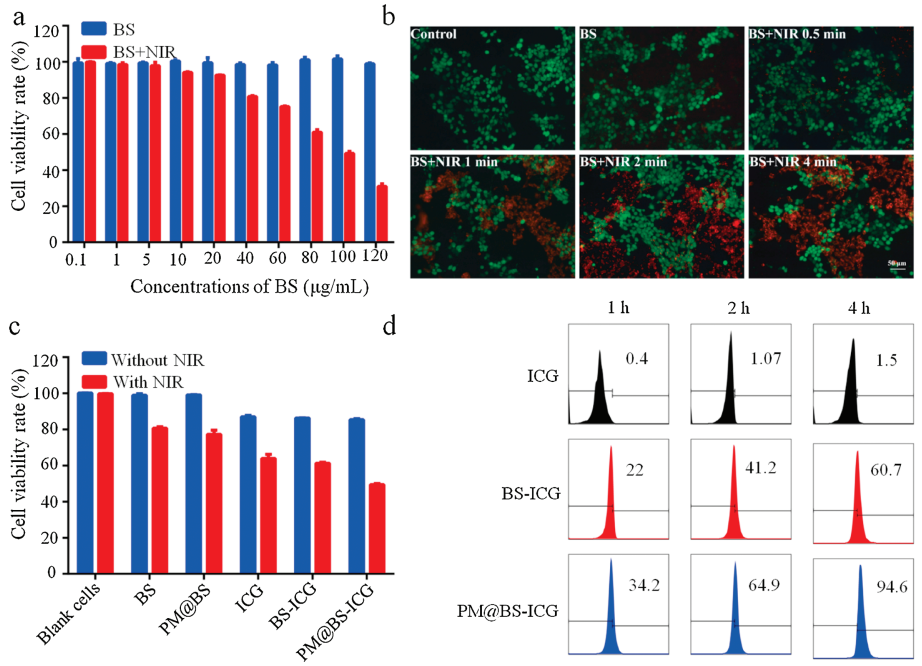

Fig. 3. (a) Cell viability of B16-F10 cells treated with BS, BS + NIR under different concentrations. (b) Fluorescence images of B16-F10 cells treated with PBS, BS, BS + NIR (0.5, 1, 2, 4 min). Viable cells were stained green with calcein-AM, and dead cells were stained red with PI. Scale bar = 50 μm. (c) The cytotoxicity of different groups with or without NIR. (d) Cellular uptake in cancer cells of different groups in preset time points detected using flow cytometry analysis.

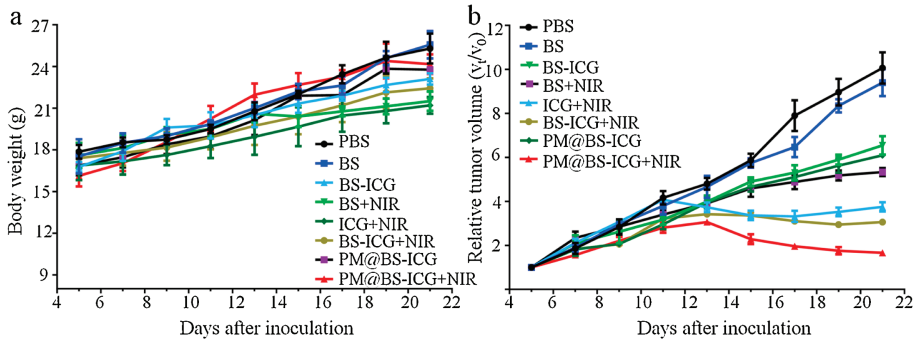

Fig. 4. (a) Body weight of B16-F10 tumor-bearing C57 mice monitored during the anti-tumor therapy period. (b) Tumor volume growth curves of B16-F10 tumor-bearing mice in different groups.

green fluorescence. The results (Fig. 3b) showed that cells cultured with BS NPs upon NIR laser irradiation presented strong red fluorescence along with the extension of exposure time, which indicated that most cells were dead.

Thereafter, we investigated *in vitro* the outstanding photothermal therapy of PM@BS-ICG NPs. Fig. 3c showed that there was no obvious toxicity on B16-F10 cells treated with BS NPs or PM@BS NPs, and the cytotoxicity of BS-ICG and PM@BS-ICG were similar to free ICG (ICG concentrations in 10 μg/mL). However, the cell viabilities of BS NPs, PM@BS NPs, BS-ICG NPs and PM@BS-ICG NPs were decreased dramatically when these groups were exposed to NIR irradiation for 2 min, respectively. Moreover, the inhibitory effect of PM@BS-ICG NPs on cells was significant superior to the other groups, respectively ($P < 0.05$). This might be due to the active tumor-targeting ability of PM and the enhancement of photothermal effects of BS and ICG.

Afterwards, the cellular uptake behavior of free ICG, BS-ICG NPs and PM@BS-ICG NPs *in vitro* was investigated through flow cytometry (Fig. 3d). The results indicated that PM camouflaging significantly enhanced the cellular uptake of BS-ICG NPs because of the targeting effect between P-selectin on the surface of PM and the CD44 receptor on the surface of tumor cells. The enhanced cell uptake of PM@BS-ICG NPs was beneficial for improving the photo-therapeutic efficiency.

For the pharmacokinetic and biodistribution analysis, the blood samples were taken out at different time after injection of ICG, BS-ICG and PM@BS-ICG (5 mg/kg for each mouse), and then the concentrations of ICG in these samples were detected using HPLC to assess the blood circulation profile. As shown in Fig. S3a (Supporting information), PM@BS-ICG group displayed longer blood circulation than BS-ICG NP and free ICG group with long circulation time ($t_{1/2\alpha} = 6.211 \pm 0.336$ h), which could be ascribed to the external PM [33,36]. The relative pharmacokinetic parameters, including area under curve (AUC), and mean residence time (MRT) of ICG for the different treatments are summarized in Table S1 (Supporting information). At 24 h after dose administration, the major organs and tumor tissues of the mice were collected to assess the biodistribution of different groups. The results were shown in Fig. S3b (Supporting information). The group coating with PM reduced the capture by liver and increased the accumulation in tumor sites, indicating that PM-coating confers the abilities of NPs to avoid phagocytosis of endothelial system and target at tumor sites, causing drug delivery systems to accumulate in tumor sites effectively.

We next assessed the anti-tumor efficacy of PM@BS-ICG NPs *in vivo*. The C57 mice bearing B16-F10 tumors were used as the mouse model, and the tumor-bearing mice were divided into 8 groups. As shown in Fig. 4a, the body weights of the mice were recorded during the treatments and no significant weight loss were observed in all groups, implying the good safety of our formulations. As shown in Fig. 4b, after 6 times of administrations, the relative tumor volumes (v_t/v_0) of PBS, BS, BS-ICG, BS + NIR, ICG + NIR, BS-ICG + NIR, PM@BS-ICG, PM@BS-ICG + NIR groups were 10.07 ± 0.58, 9.4 ± 0.5, 6.54 ± 0.35, 5.33 ± 0.15, 3.75 ± 0.17, 3.06 ± 0.07, 6.09 ± 0.04, 1.66 ± 0.10, respectively. The tumors treated with pure ICG or BS led to a weaker tumor inhibition under laser irradiation. PM@BS-ICG NPs under laser ablation showed the most powerful tumor growth suppression among all groups owing to active tumor-targeting and the enhancement photothermal effects of BS and ICG ($P < 0.05$). To further check the therapeutic effect, hematoxylin and eosin (H&E) was used to stain major organs and tumor tissues. The results were shown in Fig. S4 (Supporting information). Tumors treated with BS, ICG, BS-ICG and PM@BS-ICG under laser irradiation showed common features of thermal damage. The PM@BS-ICG group with NIR treatment led to the most enormous tumor tissue damage. But the H&E staining of major organs in PM@BS-ICG NPs groups showed no noticeable organ damage, indicating no potential toxicity *in vivo* caused by PM@BS-ICG. Our results collectively demonstrated that injection of PM@BS-ICG NPs to ablate tumor could indeed be an effective approach to promote the efficacy of PTT, without causing additional side effects to the treated animals.

In summary, we have developed PM-camouflaged hollow BS NPs loading with indocyanine green (ICG) (PM@BS-ICG NPs) for photothermal therapy. PM-based biomimetic camouflage confers the photothermal NPs with active targeting capacity and minimizes the NPs immunogenicity *in vivo*. Furthermore, upon the NIR irradiation, the rapid release of ICG together with BS significantly enhanced the efficacy of PTT. We have shown that treatment of PM@BS-ICG NPs is found to be able to remarkably enhance the tumor inhibiting efficacy of PTT, without causing notable additional side effects to the treated animals. In general, it is expected that such a strategy may have substantial potential for clinical antitumor applications and open up a versatile strategy for safe and effective cancer therapy.

Declaration of competing interest

The authors declare that they do not have any commercial or associative interest that represents a conflict of interest in connection with the work submitted.

Acknowledgments

This work was supported by the National Natural Science Foundation of China (Nos. 81673021 and U1804183), and the Scientific and Technological Project of Henan Province (No. 182102310117).

Appendix A. Supplementary data

Supplementary material related to this article can be found, in the online version, at doi:https://doi.org/10.1016/j.cclet.2019.10.040.

References

[1] Y. Zhang, R. Sha, L. Zhang, et al., Nat. Commun. 9 (2018) 4236.
[2] Q. Chen, Y. Yang, X. Lin, et al., Chem. Commun. (Camb.) 54 (2018) 5369–5372.
[3] X. Huang, Y. Yin, M. Wu, et al., Chin. Chem. Lett. 30 (2019) 1335–1340.
[4] L. Xu, F. Gao, F. Fan, et al., Biomaterials 159 (2018) 59–67.
[5] Y. Zou, W. Zhang, H. Zhou, et al., Chin. Chem. Lett. 30 (2019) 481–484.
[6] Y. Jiang, J. Li, X. Zhen, et al., Adv. Mater. 30 (2018) e1705980.
[7] A. Punjabi, X. Wu, A. Tokatli-Apollon, et al., ACS Nano 8 (2014) 10621–10630.
[8] C. Chu, E. Ren, Y. Zhang, et al., Angew. Chem. Int. Ed. 58 (2019) 269–272.
[9] F. Yan, H. Wu, H. Liu, et al., J. Control. Release 224 (2016) 217–228.
[10] P. Zhao, M. Zheng, C. Yue, et al., Biomaterials 35 (2014) 6037–6046.
[11] W. Li, J. Yang, L. Luo, et al., Nat. Commun. 10 (2019) 3349.
[12] X. Zhang, D. Li, J. Huang, et al., J. Mater. Chem. B 7 (2019) 251–264.
[13] X. Zhang, R. Zhang, J. Huang, et al., J. Mater. Chem. B 7 (2019) 3537–3545.
[14] Z. Li, J. Liu, Y. Hu, et al., ACS Nano 10 (2016) 9646–9658.
[15] H. Zhao, L. Li, J. Zhang, et al., ACS Appl. Mater. Inter. 10 (2018) 31124–31135.
[16] D. Hua, Z. Liu, F. Wang, et al., Carbohyd. Polym. 151 (2016) 1240–1244.
[17] Y. Liu, Y.J. Kim, N. Siriwon, et al., Biotechnol. Bioeng. 115 (2018) 1403–1415.
[18] A. Sánchez-Ortiz, A.G. Pérez, C. Sanz, Food Res. Int. 54 (2013) 1972–1978.
[19] M. Yu, F. Guo, J. Wang, et al., Biomaterials 79 (2016) 25–35.
[20] Y. Yu, Q. Xu, S. He, et al., Coord. Chem. Rev. 387 (2019) 154–179.
[21] D. Li, G. Zhang, W. Xu, et al., Theranostics 7 (2017) 4029–4040.
[22] L. Cheng, S. Shen, S. Shi, et al., Adv. Funct. Mater. 26 (2016) 2185–2197.
[23] G.Z. Jia, W.K. Lou, F. Cheng, et al., Nano Res. 8 (2015) 1443–1453.
[24] S. Yang, Z. Li, Y. Wang, et al., ACS Appl. Mater. Inter. 10 (2018) 1605–1615.
[25] N. Yu, Z. Wang, J. Zhang, et al., Biomaterials 161 (2018) 279–291.
[26] Z. Li, Y. Hu, K.A. Howard, et al., ACS Nano 10 (2016) 984–997.
[27] X.D. Zhang, J. Chen, Y. Min, et al., Adv. Funct. Mater. 24 (2014) 1718–1729.
[28] Z. Liu, W. Cai, L. He, et al., Nat. Nanotechnol. 2 (2007) 47–52.
[29] B.S. Zolnik, A. Gonzalez-Fernandez, N. Sadrieh, et al., Endocrinology 151 (2010) 458–465.
[30] Q. Pei, X. Hu, X. Zheng, et al., ACS Nano 12 (2018) 1630–1641.
[31] A. Parodi, N. Quattrocchi, A.L. van de Ven, et al., Nat. Nanotechnol. 8 (2013) 61–68.
[32] Z. Chen, P. Zhao, Z. Luo, et al., ACS Nano 10 (2016) 10049–10057.
[33] Q. Hu, W. Sun, C. Qian, et al., Adv. Mater. 27 (2015) 7043–7050.
[34] L. Chen, X. Zhong, X. Yi, et al., Biomaterials 66 (2015) 21–28.
[35] L. Zhang, Z. Wang, Y. Zhang, et al., ACS Nano 12 (2018) 10201–10211.
[36] D. Wu, X. Jin, X. Wang, et al., Theranostics 9 (2019) 3966–3979.